Bioinspired Fabrication and Characterization of a Synthetic Fish Skin for the Protection of Soft Materials

Natasha Funk,[†] Marc Vera,[‡] Lawrence J. Szewciw,[§] Francois Barthelat,[§] Mark P. Stoykovich,*[,‡] and Franck J. Vernerey*[,†]

[†]Department of Mechanical Engineering, University of Colorado, ECME 124, Campus Box 428, Boulder, Colorado 80309, United States

[‡]Department of Chemical and Biological Engineering, University of Colorado, C123 JSC Biotech Building, Campus Box 596, Boulder, Colorado 80309, United States

[§]Department of Mechanical Engineering, McGill University, Macdonald Engineering Building, 817 Sherbrooke Street West, Montreal, Quebec H3A 0C3, Canada

ABSTRACT: The scaled skin of fish is a high-performance natural armor that represents a source of inspiration for novel engineering designs. In this paper, we present a biomimetic fish skin material, fabricated with a design and components that are simple, that achieves many of the advantageous attributes of natural materials, including the unique combination of flexibility and mechanical robustness. The bioinspired fish skin material is designed to replicate the structural, mechanical, and functional aspects of a natural teleost fish skin comprised of leptoid-like scales, similar to that of the striped red mullet *Mullus surmuletus*. The man-made fish skin material consists of a low-modulus elastic mesh or "dermis" layer that holds rigid, plastic scales. The mechanics of the synthetic material is characterized under in-plane, bending, and indentation modes of deformation and is successfully described by theoretical deformation models that have been developed. This combined experimental and modeling approach elucidates the critical mechanisms by which the composite material achieves its unique properties and provides design rules that allow for the engineering of scaled skins. Such artificial scaled skins that are flexible, lightweight, transparent, and robust under mechanical deformation may thus have potential as thin protective coatings for soft materials.

KEYWORDS: biomimetic materials, fish skin, biomechanics, scales, thin films
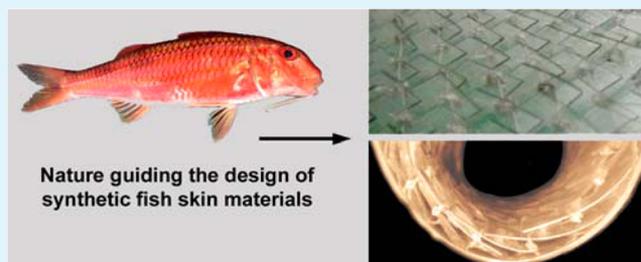
1. INTRODUCTION

Nature presents innumerable variations on armored protection systems.[1,2] Scaled skins, in particular, have remarkable mechanical properties, including being compliant, resistant to penetration, and lightweight, all of which are achieved within an ultrathin membrane structure.[3] These skins consist of discrete, imbricate (i.e., spatially overlapped) scales attached to a flexible dermis layer that accommodate the animals' motion. The skin of teleost fish, for example, provides some of the most effective protection available for its weight and flexibility.[4] At the microstructural level of an individual fish scale, there is often a mineralized exterior layer supported on a fibrillary plate of oriented collagen fibers.[5−8] This layered composite of brittle and flexible materials provides individual fish scales with a unique combination of strength, hardness, and toughness.[9−11] The overall fish skin material also achieves its mechanical and protective function because of the spatial arrangement of the scales and the interactions of the scales with the underlying dermis layer and between neighboring scales. The scales of teleost fish overlap in such a manner that the soft dermis is covered by at least three layers of scales.[4] Zhu et al. investigated the puncture mechanics of individual scales and demonstrated that the load at which complete failure of the fish skin occurs increases linearly with the number of scale layers;[4] this is similar to the linear dependence of the load to failure for single layers of homogeneous materials of increasing thickness. However, the use of overlapping but thin scales, rather than a continuous and rigid protective skin, allows fish skin to bend, stretch, and compress as required during swimming. Importantly, imbricate scales also provide redundancy if a scale were to go missing, be punctured, or otherwise be damaged.[12] In addition, each scale is secured or embedded in a "pocket" of soft tissue,[12−14] which defines the position of the scales and allows for out-of-plane scale rotation.

Although there have been recent efforts to characterize the important structural features of fish scales and fish skin (e.g., with respect to the tensile strength,[5,10,15,16] puncture strength and hardness,[4,17,18] or bending rigidity[19]), attempts to fabricate
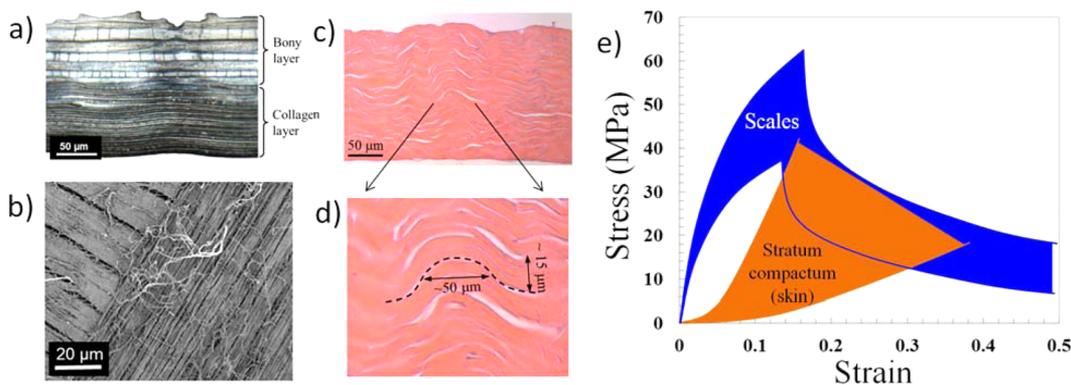
Figure 1. Scales and underlying skin for striped bass (*M. saxatilis*): (a) cross section of an individual scale showing the mineralized bony layer and collagen layer, (b) top view of a dissected scale showing a cross ply of straight fibrils, (c) histological cross section of the stratum compactum showing collagen aligned in the plane of the skin but forming crimps, (d) crimp on a bundle of fibrils, and (e) tensile stress—strain curves for scales and the stratum compactum, taking into account variations across scales, positions, and orientations. The scales are stiffer and stronger because they are partially mineralized and the constituent fibers are straight.

materials that mimic the structural and mechanical aspects of natural fish skins have been limited. Ortiz, Boyce, and co-workers[13] explored the mechanics of fish scale composites by fabricating three-dimensional (3D), macroscale prototypes using printed thermopolymer scales embedded in an elastic substrate of silicone rubber. The distribution of forces across the material during indentation, via deformation mechanisms, including scale bending, scale rotation, and substrate shear, influences the overall stiffness of the material and can be tuned through structural parameters such as the scale overlap, orientation, aspect ratio, and volumetric filling within the substrate.[13] Other 3D-printed prototypes based on the armor of *Polypterus senegalus*, from an ancient family of fish with rigid ganoid scales, have been used to characterize the global and local behavior of scaled skins. With these models, it was demonstrated that flexible "peg-and-socket" connections in combination with sliding, overlapped scale surfaces were critical to mobility in *P. senegalus*.[20,21] Dry transfer printing techniques have also been applied to fabricate layers of microsized (600 μm × 600 μm × ~3 μm) imbricate scales on flexible and stretchable substrates.[22] The scales were Si-based, sourced from wafers, and demonstrated to provide high-performance optoelectronic functionality; however, in this instance, the ultrathin scales do not contribute significantly to the mechanical response of the overall material. The scales provided full coverage and protection during bending, stretch, and buckling deformations, thus making such material layouts attractive for the development of flexible electronics. Chintapalli et al.[23] recently built a synthetic model material that mimicked some of the features of natural scales and osteoderms. Their system consisted of hexagonal glass plates resting on a substrate that was softer than the plates by several orders of magnitude. It was demonstrated that in addition to providing flexural compliance and damage tolerance, the bioinspired segmented design also increased the puncture resistance by up to 70% compared to that of a continuous plate of the same protective material. Although these modern designs share structural aspects and duplicate some performance features of natural materials, such man-made materials have yet to fully capture key features of the fundamental mechanics in fish skin.

2. THE MAIN CHARACTERISTICS OF SCALED SKINS OF FISH AND OTHER ANIMAL SPECIES

The scaled skins of fish and other armored animals are complex systems with multiple levels of structural hierarchy and can vary in size, composition, and structure across species. Two characteristics, however, are common to all scaled skins. (i) The protective material is several orders of magnitude stiffer than the underlying tissues, and (ii) the hard material is segmented into multiple plates. Segmented hard plates can resist puncture and at the same time are able to move relative to each other. This approach therefore solves the design contradiction of protecting the animal (soft tissue) against sharp puncture (which requires hard materials) while maintaining the flexural compliance necessary for unhindered motion (which requires soft materials). Figure 1 illustrates the first of these characteristics for striped bass (*Morone saxatilis*).

Individual scales consist of collagen type I partially mineralized with hydroxyapatite, which is concentrated in the outer layer of the scale (bone layer, Figure 1a). A top view of a dissected scale (Figure 1b) reveals straight collagen fibrils forming a cross ply structure with the fibrils aligned with the plane of the scales. The skin underneath the scales, termed the stratum compactum, is also mainly composed of collagen type I, but with a different microstructure. The fibrils are crimped, with a wavelength and an amplitude of ~100 and ~15 μm, respectively (Figure 1c,d). Figure 1e shows the stress—strain curves of the scales and stratum compactum as measured in tension. For each material, the colored domain represents the range of measured stress—strain curves, resulting from variations associated with different orientations, the sample position, and other biomechanical variations. The scales are relatively stiff and display a linear elastic behavior followed by progressive softening and failure past the maximal stress. In contrast, stratum compactum displays an elastomeric type of response with a very soft initial modulus, followed by nonlinear elasticity and stiffening until sudden failure. The softer response of the stratum compactum and the initial low stresses associated with deformation can be explained by the uncrimping of the fibers, a phenomenon also found in other collagenous tissues such as tendons.[24] In contrast, the straight fibers in the scales provide a stiff response as soon as they are stretched, and their stiffness and strength are further increased by the mineral they contain.
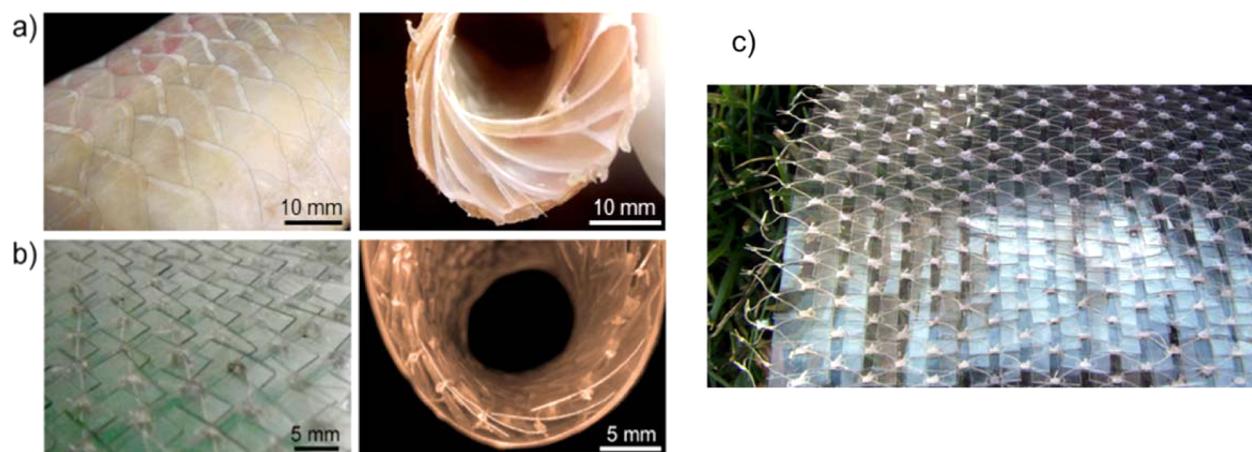
Figure 2. Photographs of the skin of (a) the striped red mullet (*Mullus surmuletus*) and (b) the synthetic material when undeformed (left) and under a bending deformation (right). (c) The synthetic fish skin specimen fabricated and characterized in this work consisted of 690 scales and covered an area of ~154 mm × 168 mm.
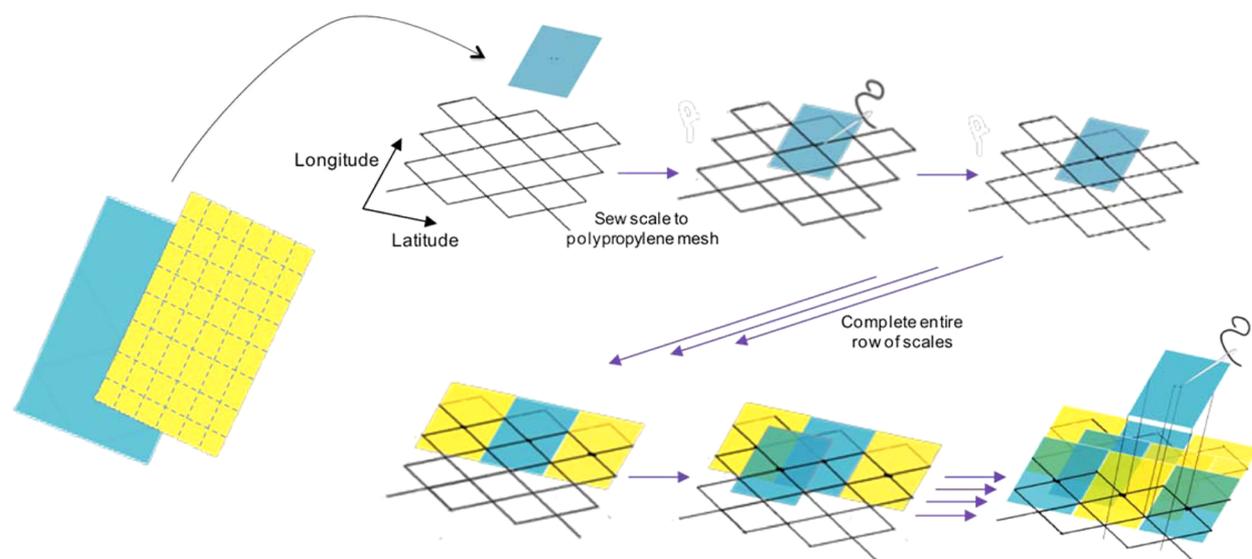
Figure 3. Schematic of the fabrication process for the synthetic fish skin material. A 90 mm × 60 mm sheet of cellulose acetate butyrate (CAB) (shown as blue and yellow sheets to distinguish individual scales) was cut into small rectangular scales (9.5 mm × 12.7 mm) whose dimension was controlled by the dimensions of the available mesh. After each scale was fabricated, two small adjacent holes were punched into the center of the scales in preparation for fastening them to the mesh. A polypropylene mesh or netting (represented by the black diamond pattern) was purchased, and scales were then inserted through an opening in the mesh, such that one-half of the scale rested on top of the mesh and the other half rested under the mesh. The premade holes were aligned with the mesh node, and cotton thread was used to attach the scale to the node with three stitches and a single knot. This process was repeated by hand for each node on the mesh.

3. A NEW SYNTHETIC FISH SKIN

Here we report a man-made or synthetic fish skin material (Figure 2) designed to replicate the structural, mechanical, and functional aspects of natural teleost fish skin comprised of leptoid-like scales, such as that of *Mullus surmuletus* or the striped red mullet. Flexible and lightweight scaled skins found in teleost fish allow for the bending and rotation of individual scales, more so than materials based on *P. senegalus*, under varying modes of deformation. The material design and fabrication have been simplified to include the key characteristics of a low-modulus elastic mesh or "dermis" layer that holds relatively rigid (in comparison to the mesh) plastic scales. While the role of the mesh is to provide in-plane elasticity and to hold the scales in place as the material is deformed, it also provides a mechanism by which scales can rotate and interact

with adjacent scales. As demonstrated in the tests and models described below, the mesh, when placed in uniaxial tension, can reorient its structure and provide a stiffening response similar to that of the stratum compactum shown in Figure 1. After fabrication, the mechanics of the resulting material in response to in-plane deformations, bending deformations, and indentation was experimentally characterized and analyzed with theoretical models. The mechanical behavior achieved with this design was found to be similar to that of natural teleost fish skin, thus highlighting the distinct roles that interacting dermal and scale layers have on the composite material properties. Overall, the synthetic fish skin is flexible and can conformably cover a range of surfaces, including those subject to diverse modes of deformation, making it attractive as a low-weight, low-profile protective coating for soft materials.
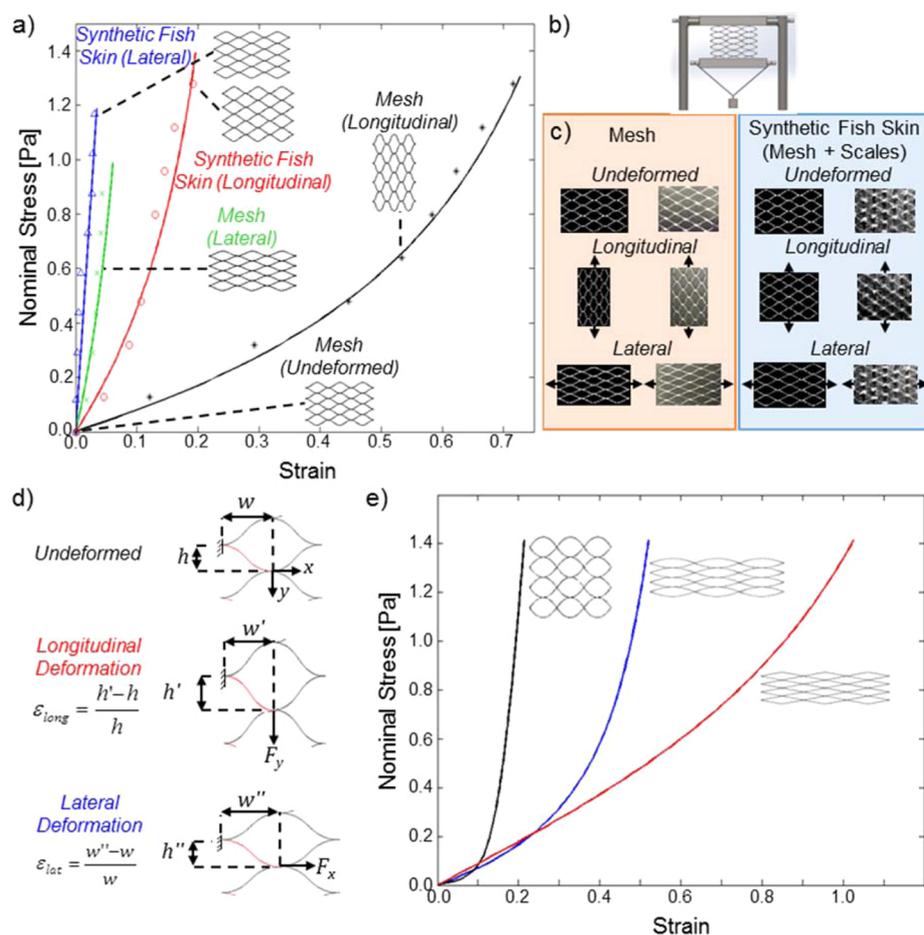
Figure 4. Mechanical response of the bioinspired fish skin material under in-plane deformation. (a) Stress–strain response of the synthetic fish skin material and components to tensile deformation as characterized by experiments (discrete data points) and the mechanics model (solid curves). The synthetic fish skin under lateral and longitudinal tension is colored blue and red, respectively, while the lateral and longitudinal response of the mesh only is colored green and black, respectively. (b) Schematic of the experimental tension setup. (c) Comparison of the model predictions (images at left) and experimental observation (photographs at right) of the elastic mesh under tension for the mesh only and the synthetic fish skin (mesh and scales). (d) Free-body diagram used to model the tensile deformation of the elastic mesh. Because of the periodic configuration of the mesh, responses were calculated for a unit cell as shown in red and then tiled appropriately. Stress was calculated as $\sigma_x = F_x/h'$ or $\sigma_y = F_y/w'$. (e) Model predictions for the longitudinal (horizontal in the figure) stress–strain responses of meshes with different geometries (initial, undeformed geometries shown in the insets).

Prior research into the architecture of fish skin has indicated some components that are key to the mechanical response of natural fish skin: (1) thin but relatively rigid scales with some degree of spatial overlap, (2) an underlying elastic substrate or dermis, and (3) a periodic distribution of soft, elastic pockets in the substrate into which the scales are inserted.[12,13] A simplified bioinspired skin was fabricated, using the process shown in Figure 3, from two primary materials that included a flexible polypropylene mesh to reproduce the functions of the dermis and a number of overlapping small plates made of cellulose acetate butyrate (CAB) to mimic the scales. As in natural fish skin, the mesh serves the dual purpose of providing both a relatively soft, flexible scaffold (the overall mesh has an elastic modulus that is ~7 orders of magnitude lower than that of the scales) and a "pocket stiffness" that allows the rotation of individual scales about the lateral axis [dorsal to ventral direction on the fish (see Figure 2)] while resisting rotation about the longitudinal axis (head to tail direction on the fish). This periodic mesh also controls the scale position, spatial overlap, and thus the scale–scale interactions. Structurally, the mesh consists of periodically repeated, sinusoidal fibers that

have an elastic modulus of 1300 MPa[25] and a radius of 0.06 ± 0.01 mm. The dimensions of the fiber segments between nodes in the mesh were 5.13 ± 0.01 and 2.81 ± 0.01 mm in the lateral and longitudinal directions, respectively, creating diamond-shaped openings measuring 10.26 ± 0.01 mm wide by 5.62 ± 0.01 mm tall (see Figure 3). The CAB scales were attached at their center to the nodes of the mesh with cotton thread in a row-by-row manner as indicated in Figure 3. While natural fish scales are not attached to the underlying dermis at their center, it was found that this method of attachment allowed individual scales to overlap, rotate, and interact in a manner very similar to that of real fish skin. The individual scales have an elastic modulus of 800 MPa, a thickness of 0.20 ± 0.01 mm, a width of 9.46 ± 0.01 mm, a length of 12.68 ± 0.01 mm, and a normalized overlapping ratio (r defined as the ratio of scale spacing to scale length) of 0.19, which is similar to values found in nature (typically r is between 0.2 and 0.3 for teleost fish).[12] The length and width of the scales were controlled by the available mesh, and the effects of scale size on the overall mechanical characteristics of the material were not explored.

A macroscopic specimen consisting of 690 scales (see Figure 2c) and spanning an overall area of 153.39 ± 0.01 mm in the lateral direction by 167.87 ± 0.01 mm in the longitudinal direction was fabricated, and its mechanics was characterized using standard deformation tests. As compared in panels a and b of Figure 2 (left panels), the synthetic fish skin material has an imbricate layout similar to that of the striped red mullet. Upon bending (right panels in panels a and b of Figure 2), the scales of the natural fish skin and the man-made material begin to rotate and eventually interact, thus inducing bending of individual scales. The following sections compare the observed mechanics of the synthetic fish skin material to theoretical deformation models, thereby elucidating the critical mechanisms by which the composite material achieves its unique properties and providing design rules that permit the engineering of thin, protective coatings.

4. IN-PLANE DEFORMATION

The mechanical response of the bioinspired fish skin material was first characterized under in-plane strains, the experimental results and theoretical predictions of which are shown in Figure 4.

4.1. Testing. The response of the fish skin was compared to those of two reference materials: the polypropylene fiber mesh used for the dermis layer (i.e., devoid of scales) and a continuous, solid sheet of CAB with a thickness identical to that of the scales. Tensile tests were thus performed on three separate materials: the polypropylene mesh, the synthetic fish skin material (mesh and scales), and a double layer of CAB sheets. We decided to compare the synthetic fish skin to a double layer of CAB rather than a single layer because in its at-rest state, the synthetic fish skin is approximately two scale layers thick. During testing, the upper end of the specimen was attached to a smooth metal rod every 10 mm along the edge of the material. The free end was then attached to a smooth metal rod in the same manner. The upper rod was then placed between two supporting beams near a smooth, vertical surface to reduce any out-of-plane deformation (see Figure 4b). Loading was then performed manually in increments of 0.2 N, and deflection was measured at the center point of the specimen after the application of each load. The fish skin material was not loaded to failure; thus, the original shape and properties were recovered upon unloading. Deflection was measured using electronic calipers only after the specimen had reached the steady state, and care was taken to prevent the mesh from interacting with the vertical surface. The tensile responses of the anisotropic materials (i.e., the synthetic fish skin and the mesh) were measured in the longitudinal and lateral directions as shown by discrete points in Figure 4a; the deformation of the sheet of CAB was negligible for this range of loadings and is not shown.

4.2. Model. To better understand the mechanisms by which the synthetic fish skin deforms, a simple numerical model was developed for the in-plane deformation of an elastic mesh with and without scales. Briefly, an idealized mesh (Figure 4c) was modeled displaying the same overall diamond-like openings as the actual mesh. The deformation of the mesh under loading was then computed numerically using a finite element formulation of the finite deformation/rotation of the fibers.[26] More specifically, when the periodic geometry of the mesh was noted, the response of the mesh was determined numerically by placing kinematic boundary conditions on a single polypropylene fiber as shown in Figure 4d and computing the conjugate

forces. The modeled fiber, or beam, had an elastic modulus of 1300 MPa and a circular cross section with a radius of 0.21 ± 0.01 mm. Shear effects were neglected because the beam was very long in comparison to its thickness. The undeformed geometry of the beam (as shown in red in Figure 4d) along its length was modeled as a third-order polynomial. To implement the problem of finite deformation of fibers in this unit cell, the beam was divided into 40 finite elements. At each increment of loading, the stress on the fiber was calculated as the applied force divided by the effective mesh width w (longitudinal deformation) or length h (lateral deformation) as denoted in Figure 4d:

$$\sigma_{long} = \frac{F_y}{w'} \quad \sigma_{lat} = \frac{F_x}{h''} \tag{S1}$$

Similarly, the strain was computed by dividing the change in effective mesh length or width by the undeformed length h (longitudinal deformation) or width w (lateral deformation). This method of computing stresses and strains effectively normalized the response of the mesh to the unit cell shown in Figure 4d, which allowed for a direct comparison between the model and the experimental results as in Figure 4a. This method was then extended to model the stress−strain response of the skin by idealizing each scale as a spring separating the nodes of the mesh in the lateral direction. Note that this stiffness represents an effective measure of the interaction between scales and the fiber during lateral contraction. Its value was therefore adjusted to match the value of a macroscopic Poisson ratio of 0.35. Eventually, this constraint resulted in increasing the tensile stiffness and reducing the Poisson's ratio of the bioinspired skin compared to that of the mesh without scales.

4.3. Results and Interpretation. We found that this simple deformation model successfully predicts the responses of the fish skin and the mesh in both the lateral and longitudinal directions, as shown in Figure 4a (solid curves), thereby providing insight into the mechanisms by which the material design controls in-plane deformation. Specifically, the in-plane tensile measurements provided four notable observations. First, the skin shows a relatively soft and strain-stiffening response in the longitudinal direction (i.e., the resistance to deformation increases with increasing strain). Second, comparison of the longitudinal responses of the mesh and the skin indicates that the presence of scales increases the stiffness of the skin by constraining lateral strains (i.e., strains in the x direction as labeled in Figure 4d). This mechanism holds true in the lateral direction as well and can be quantified by comparing the effective Poisson ratios of the mesh and the skin in both the longitudinal and lateral directions (see Figure 4d for strain equations). For a specific longitudinal strain of 0.2, the following Poisson ratios were computed:

$$\nu_{long,mesh} = -\frac{\varepsilon_{trans,long}}{\varepsilon_{axial,long}} = 0.35, \quad \nu_{lat,mesh} = -\frac{\varepsilon_{trans,lat}}{\varepsilon_{axial,lat}} = 0.26$$

$$\nu_{long,scales} = -\frac{\varepsilon_{trans,long}}{\varepsilon_{axial,long}} = 0.25, \quad \nu_{lat,scales} = -\frac{\varepsilon_{trans,lat}}{\varepsilon_{axial,lat}} = 0.14$$

The axial strain is the strain computed with respect to the direction of loading, and transverse strain is computed perpendicular to loading. For example, for the longitudinal test, ε_{long} represents the strain in the axial direction, $\varepsilon_{axial,long}$, while ε_{lat} measured during this same test represents the strain in
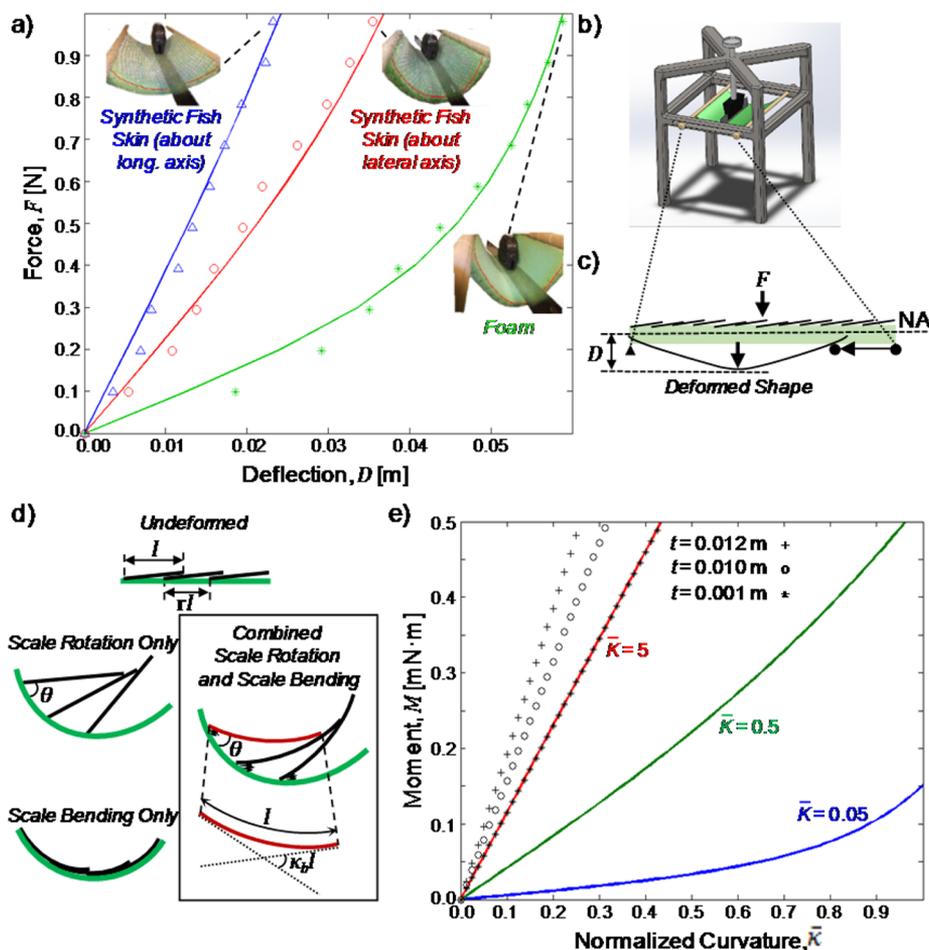
Figure 5. Mechanical response of the bioinspired fish skin material to flexural deformation. (a) Force−displacement response of the synthetic fish skin material and components to bending as characterized by experiments (discrete data points) and the mechanics model (solid curves). Bending of the synthetic fish skin was considered about the longitudinal (blue data) and lateral axes (red data), as was bending of the foam substrate (green data). (b) Schematic of the experimental flexural setup. (c) Free-body diagram used to model the bending response. The supports were allowed to move freely, and the deformation was measured at the midpoint of the specimen. (d) Schematic of the rotation and bending responses observed in individual scales when the skin is flexed. (e) Effect of the normalized pocket stiffness $\bar{K} = Kl/(EI)_s$ and substrate thickness t on the moment of the synthetic fish skin as a function of the normalized curvature.

the transverse direction, $\varepsilon_{\text{trans,lat}}$. It was found that the observed Poisson effect was the result of the realignment of fibers in the direction of stretch, which induce a lateral contraction of the mesh. This phenomenon is therefore mostly governed by the geometry of the mesh and the direction of stretch with respect to the principal directions of the mesh. Furthermore, because of the nonlinearity of the material's response exhibited in Figure 4, these values are expected the change with deformation while the trends will remain the same. Interestingly, to the best of our knowledge, this phenomenon has not been reported in the literature, and it would be worthwhile to investigate whether this behavior is also observed in natural fish skins. Third, the response of the skin is clearly anisotropic. In the longitudinal direction, the scales provide very little resistance to strain, because the geometry and structure of the skin allows for the scales to slide across each other freely. In contrast, the scales are restricted from sliding in the lateral direction. Ultimately, these mechanisms allow the mesh to dictate the general response of the skin during stretch.

The final notable observation is that the in-plane strain-stiffening behavior is fully controlled by the geometry of the mesh, which dictates when fiber deformation undergoes the transition from a soft bending mode to a stiffer tensile mode. Figure 4e demonstrates the use of the model for designing a mesh or dermis layer with the desired tensile response for the synthetic fish skin material. Three distinct mesh geometries (the undeformed meshes are shown in the inset images), but with identical fiber dimensions and physical properties, were considered and exhibited significantly different mechanical responses when placed in tension in the longitudinal direction. Conceivably, the mesh geometry can be used as a design parameter to control the anisotropy of the skin and the linearity of its behavior and to achieve an optimal balance between stiffness and flexibility.

5. FLEXURAL DEFORMATION

The presence of scales on the skin affects the material's mechanics during out-of-plane deformation as arises during bending and indentation by a sharp object. For example, the relatively high curvatures of the skin achieved when a fish is swimming serve a mechanical function, as the skin acts as a spring to restore elastic energy and assist in more efficient propulsion.[19,27] Imbricate scales also play an important role in protection when the skin is subjected to extreme surface

instabilities such as wrinkling of the skin (from pinching and/or buckling) or sharp indentation.

5.1. Testing. To characterize the response of the synthetic skin under bending, we considered a two-layer system made of a thick porous polyurethane foam layer, mimicking the role of a substrate or the underlying soft tissue of a fish, covered by the scaled skin layer described above. The flexural response of the structure was then characterized with a three-point bending test, during which the two opposite sides of the material were stitched to long rods with circular cross sections. The rods were then laid on parallel supporting beams which allowed them to freely move closer to one another as a line load was applied parallel to their long axis, directly on the center of the specimen. After the load was applied, the specimen was allowed to settle before a deflection measurement was taken at the point of loading. Loads were applied incrementally at the center of each specimen using the testing setup illustrated in Figure 5b,c). The flexural tests were performed in both the lateral and longitudinal directions for the anisotropic fish skin material. For those specimens consisting of two materials, i.e., the scaled skin on a foam substrate and the "solid CAB + foam" specimens, the protective material was stitched every 10 mm along the edges of the foam using cotton thread. No attachments were made within the center portion of the foam.

Figure 5 reports the flexural response of the synthetic fish skin material on a foam substrate about both the lateral and longitudinal axes. The load-deflection responses (Figure 5a) of the skin were compared to those of an unscaled (or unprotected) foam substrate (i.e., analogous to the flesh of a fish). It is found that the synthetic skin increases the overall flexural stiffness of the foam substrate but that this contribution becomes less significant for high curvatures. The flexural response of the fish skin material did not display any hysteresis upon cyclic loading and unloading. However, it was observed during testing that at the maximal load, the unscaled foam specimen displayed a buckling-like instability at higher curvatures (as indicated by a kink at the point of loading), whereas the same foam specimen, when protected by the scaled skin, did not display such an instability.

5.2. Model. To gain further insight into the bending of scaled skins, we have developed a numerical model that connects mechanical behavior to structural features that include the mechanical properties, spatial organization, and morphology of individual scales. The model is based on the decomposition of the elastic energy stored in the skin into components that are associated with scale bending and scale rotation as illustrated in Figure 5d (separately and combined), and that is observed in the natural and synthetic fish scales in Figure 2. The rotational energy arises from the presence of the skin pockets that act as springs (of stiffness K) that resist the out-of-plane scale motion. Because of the relatively low modulus of these pockets, scale rotation is dominant at low bending deformations. However, as curvature increases, individual scales begin to bend because of their interactions with adjacent scales, resulting in a stiffening of the flexural moment. A similar model[12] has been used previously to show that the internal moment can be computed as $M = [(\text{EI})_s/(rl)][\overline{\kappa} - \overline{\kappa}_r(\kappa)]$, where $(\text{EI})_s$ is the bending stiffness of the scales, r (the ratio of scale spacing to scale length) and l (length of a single scale) are the geometric parameters as specified in Figure 5d, and $\overline{\kappa}$ and $\overline{\kappa}_r$ are the total normalized curvature and the normalized curvature generated by scale rotation, respectively. Here we have extended the model to investigate the finite deformations of the composite skin composed of a thin upper scaled layer and a thick underlying polyurethane foam. The full derivation of this model is provided in the Appendix. In the model, boundary conditions were specified to allow free motion in the horizontal direction as well as free rotation, while restricting displacement in the vertical direction (identical to the experimental setup as drawn in Figure 5c). The flexural stiffness associated with the open-celled, polyurethane foam (153.39 ± 0.01 mm $\times$ 167.87 ± 0.01 mm $\times$ 11.99 ± 0.01 mm) was computed on the basis of a tensile modulus of 0.06 MPa and a compressive modulus of 0.02 MPa.

5.3. Results and Interpretation. The mechanics model (solid red curve) was successfully fit to the empirical data (discrete points) as shown in Figure 5a, thereby indicating the importance of these scale-level deformation mechanisms in the overall response of the fish skin material. When the scales in the model were removed [i.e., by setting $(\text{EI})_s = 0$], a response was generated for the case of the unscaled foam (solid green curve in Figure 5a), which also closely matches the measured experimental data. In contrast, the bending response about the longitudinal axis does not involve scale rotation (only bending) and may therefore be modeled as a layered beam composed of the foam substrate covered with a solid CAB layer. A good match with the experimental results (solid blue curve in Figure 5a) was achieved for an effective CAB thickness of 0.64 mm, which represents ~3 times the thickness of the single layer of CAB used to create the synthetic scales. The effective scale thickness can be calculated as $t_{\text{eff}} = nlbh/LW$, where n is the number of scales on the specimen and l, b, and h are the length, width, and thickness of a single scale, respectively. L and W are the length and width of the foam specimen, respectively; thus, LW indicates the area covered by the fish skin.

From this mechanical characterization, the following conclusions may be drawn. First, the scaled skin behaves softly in the longitudinal direction (bending about the lateral axis) in comparison to a solid sheet of CAB of equal thickness (35.5 mm of deflection in comparison to 21 mm of deflection at a load of 1 N) attached perfectly to the foam specimen. The mechanism controlling this soft behavior is the small rotational stiffness of the scale pockets, which allows for large scale rotation rather than individual scale bending under relatively low applied moments. At larger bending moments, however, the skin stiffened significantly with curvature and scale–scale interactions led to individual scale flexure. Furthermore, in the lateral direction (bending about the longitudinal axis), it was observed that the skin also responded more softly than a solid sheet of CAB of equal thickness, which can be explained by the discontinuity of material across the surface of the skin. Contrary to the behavior in the longitudinal direction, however, the limitation on scale rotation restricts overall bending of the skin in the lateral direction, leading to a stiffer response and eliminating the strain stiffening behavior seen in the longitudinal direction. This overall stiffer behavior can also be attributed to the fact that the flexural stiffness of a single scale, EI_s, is larger about the longitudinal axis because the scales are longer than they are wide and $I_s = lh^3/12$. These results display the two-dimensional flexibility of the synthetic specimen in comparison to a solid sheet of protective material.

The proposed bending model successfully describes the empirical observations, indicating that this model has the potential to also be used for the design and optimization of synthetic scaled skins. In Figure 5e, the model is extended to explore two approaches that may be used to influence the skin's
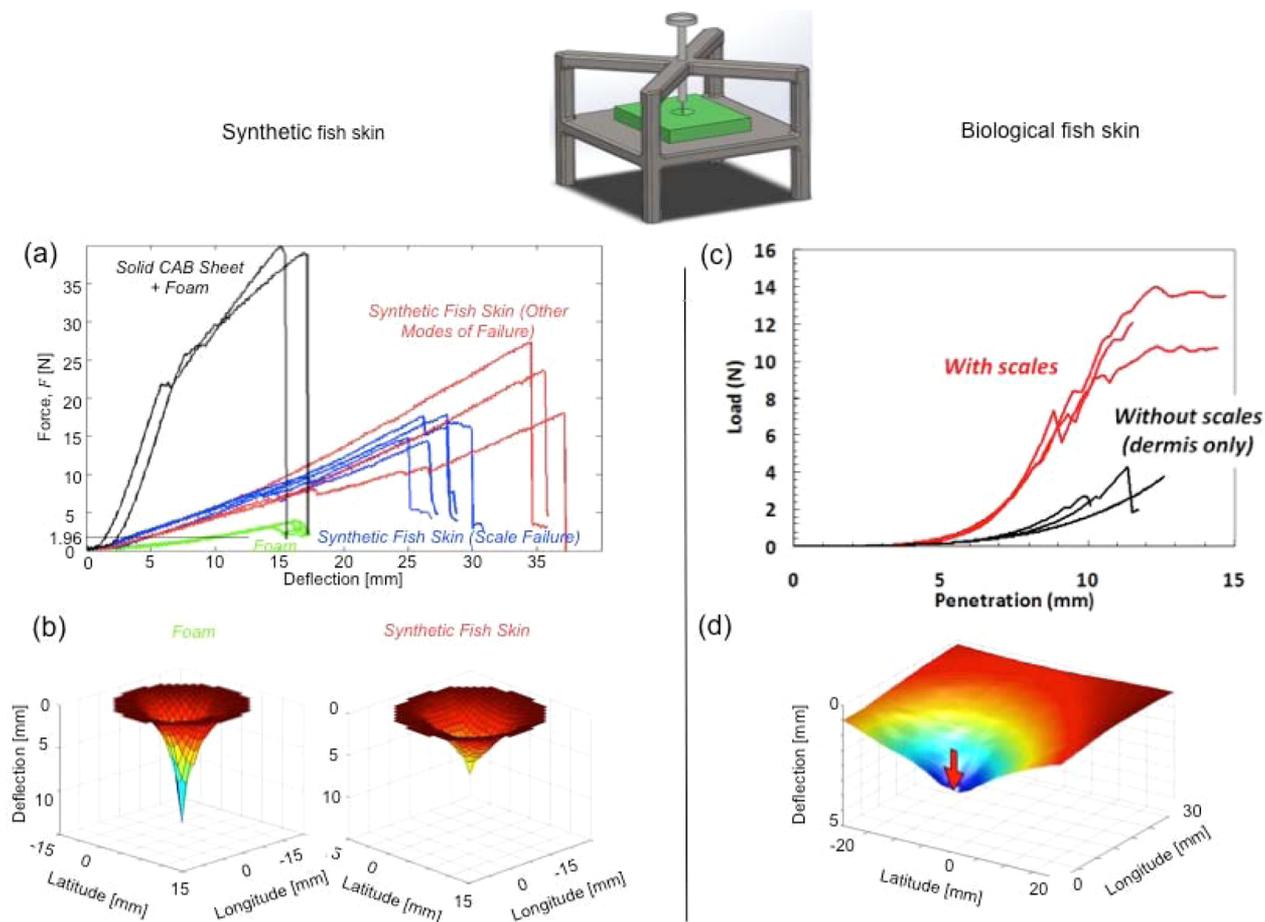
Figure 6. Resistance of bioinspired synthetic (left) and real fish (right) scaled skin materials to indentation. (a) Puncture resistance of the synthetic fish skin as measured by indentation. "Scale failure" indicates the direct puncture of a scale, whereas "other modes of failure" of the synthetic material considers failure of the mesh or buckling of a scale. (b) Contour surfaces of the synthetic fish skin deformed under a static load of 1.96 N (just below the critical load of the foam). (c) Load-deflection curves from the indentation of the dermis of the striped bass with and without scales and (d) an associated deflection profile.[4]

bending response in the longitudinal direction: (1) tuning pocket stiffness and (2) controlling substrate thickness. The effect of pocket stiffness is considered by removing the foam substrate from the model (specifically achieved by setting t_{foam} to 0). These results are shown as solid curves in Figure 5e, where it is noted that an increase in normalized pocket stiffness, $\bar{K}$, leads to an increase in skin stiffness and a reduction of the stiffening response at higher curvatures. The blue curve [$\bar{K}$ = 0.05 (far right)] demonstrates the effect of low pocket stiffness, which causes the overall skin to be much more flexible initially than a similar specimen with high pocket stiffness. The discrete points in Figure 5e represent the scaled substrate as modeled in Figure 5a, only with varying values of substrate thickness as specified within the plot. It is noteworthy that adding the foam substrate increases the stiffness of the specimen such that the pocket stiffness no longer has an effect on the overall response of the skin. With this type of modeling capability, it would be possible to optimize or customize the response of the synthetic skin based on the desired application of the material.

6. RESISTANCE UNDER INDENTATION

In nature, a crucial function of scaled skins is to provide resistance to penetration.[4,9] The same parameters of scale rotation and scale bending that control the skin's response to flexure also influence its response during indentation.[28]

However, another important characteristic controlling the indentation response is the imbricate pattern of the scales. The overlapping of scales allows for the transfer of load applied to a single scale to the scales directly adjacent, dispersing the force over a larger area and ultimately decreasing localized damage to the underlying tissues. For example, indentation tests on skins of *M. saxatilis* using a sharp needle (35 μm tip) demonstrated that scaled skin was able to resist approximately 3 times the penetration force as a comparable unscaled skin.[4] The puncture resistance was roughly proportional to the number of scales punctured. These prior experiments were performed on natural fish skin, where the scalation pattern is such that three scales overlap at any point on the surface. Individual scales are the thickest in the center, and as a result, the centers of the scales have the highest resistance to puncture. However, scales in natural skin overlap in such a way that the total thickness of scales remains uniform across the surface.[4] It was also established that the friction coefficient between the natural scales is negligible during indentation and scale bending. Finally, under blunt loading (a probe diameter of 2.2 mm), the scales reduced the absolute deflection by interlocking and redistributing the force across the skin.[4]

6.1. Testing. To characterize the response of the synthetic fish skin under puncture, we therefore performed a series of indentation tests with an Instron 5869 Universal Testing

Machine. Two types of indentation tests were performed with a cylindrical indenter with a radius of 1.14 mm, which is more than 8 times smaller than an individual scale.

6.1.1. Quasi-Static Loading until Failure. This indentation test was performed at a slow loading rate of 0.1 mm/s, for which the material's response was unaffected by the loading rate. The tests were performed until rupture, and the force/deflection curves are reported in Figure 6a.

6.1.2. Static Test. For each specimen, a static indentation test was performed three times. Each time, the load was applied to the specimen at least 30 mm from its edge to avoid possible boundary effects. The shape of the deflected region was then determined by measuring the vertical displacement of points on the skin (at 1 mm intervals from the origin, i.e., the indentation point) with respect to a reference plane located on top of the specimen. Points were distributed in a radial pattern every 30°, giving a total of 168 measurements for each test. This test allowed an understanding of the local material deformation around the point of puncture, for the skin and control specimens consisting of a solid sheet of CAB (two layers of CAB with the same total thickness as the scales in the synthetic skin) and the unscaled foam substrate. The resulting surface contours are plotted in Figure 6b.

6.2. Results and Interpretation. Figure 6a shows that the synthetic fish skin has increased resistance to penetration compared to unscaled specimens, thus allowing greater loads and displacements to be applied prior to indentation (∼7 times the failure load of the foam substrate). The scales also have the added benefit of flexibility (i.e., soft responses in tension and bending) relative to the solid sheet of CAB and thus display a higher deflection at similar loadings. Using the same indenter, the materials were also indented at a static load of 1.96 N, which is slightly below the critical static load for the unscaled foam substrate. The scales reduce the localized deformations by dispersing the applied load over a large area (∼30 mm in diameter). This behavior results, in part, from the nonlinear bending mechanisms (e.g., strain stiffening) detailed above and is also a function of the individual scale size.[28] At small applied loads, the scale(s) directly in contact with the indenter transfers the load to neighboring scales through the mechanism of scale rotation. As the displacement increases, the localized curvature also increases and, just as in the case of bending, individual scales begin to bend and stiffen the response of the material. The distribution of forces depends directly on the size of the scales, with larger scales distributing the forces over larger areas. As an extreme example, the solid CAB sheet may be considered to be a very large scale, and it is found that the solid sheet disperses the force over an area much larger than the area of the fish skin material and is not significantly (∼1 mm) deflected. Likewise, if we were to imagine that the scale size was infinitely small compared to the indenter size, we would see a response similar to that of the unscaled foam substrate, which does not effectively disperse the applied load and creates a situation prone to failure nucleation and penetration.

For comparison, we also show, in Figure 6c, a set of representative load-deflection curves obtained from a sharp indentation test on striped bass (*M. saxatilis*). The force to puncture natural scales is lower than that for the synthetic scales because the materials and dimensions are different, but the overall shape of the curve is similar: initial stages of indentation are characterized by stiffening, followed by softening as the scales progressively fail. Figure 6d shows how the deflection of the scaled skin around the indenter is also

well distributed around the sharp point load due to the collective contacts between the scales (which are ∼10 mm in diameter in this case). This effect is also similar to what is observed for the synthetic fish skin (Figure 6b).

Generally, because of the flexibility of the overall skin and the puncture resistance of individual scales, the mechanical work that needs to be expended to puncture the skin (the area under the force-deflection curve) is significantly increased compared to the substrate alone. It is found, however, that the synthetic skin displays a peak stress that is less than that of two layers of CAB. Such a result differs from a similar analysis of scaled materials presented previously.[23] This relative skin weakness stems from different origins, in particular the general fabrication technique and choice of scale material. Indeed, two primary failure modes were observed during indentation: scale failure and mesh failure. Scale failure occurred when the indenter punctured a single scale, while the adjacent overlapping scales rotated around the indenter. In this case, failure was related to the failure of a single, instead of the double, scale layer explaining the reduction in peak stress by almost one-half. This issue could potentially be addressed by restricting the relative motion of scales when they are subjected to high normal forces. For instance, sliding of scales past each other could be inhibited by increasing the surface rugosity or roughness of the scales, in a manner analogous to the microridges observed in natural fish scales. On the other hand, mesh failure encompassed the failure of individual fibers or scale buckling, which occurred when a scale folded upon itself and was pushed through the mesh. We note here that this mode of deformation was due to the relatively weak mesh material that was used for our study. In comparison, failure at points of attachment of scales to the mesh (the cotton thread) was not observed, and the load transferred to the scale attachments was lower than their failure point. Better designs, in the future, should thus focus upon a stronger mesh material (e.g., from lightweight fibers of Kevlar[29] or carbon nanotubes[30,31]) to postpone fiber fracture during indentation. A solution based on modifying the shape of the scales (to prevent scale buckling and being pushed through the mesh) or increasing the flexural strength of the scales may also be considered.

7. CONCLUSIONS

In summary, we have fabricated a biomimetic fish skin material using a simple design and inexpensive materials. The design principles and materials that were discovered are compatible with conventional fabrication processes across the macro- and microscales, including via photolithography or printing techniques, such that the automated and high-throughput production of synthetic scaled skins may be envisioned. Via characterization of the mechanical response of this material during in-plane deformation, flexure, and indentation, the synthetic fish skin has been proven to possess many of the advantageous attributes of its biological counterpart, highlighting its potential for providing the unique and attractive combination of flexibility and protection found in natural materials. The overlap of the scales, the underlying mesh geometry, and the mechanical properties of the constitutive materials contribute significantly to the overall mechanical behavior of the synthetic fish skin material, including a unique strain-stiffening response. Fortunately, as developed here, simple models of deformation mechanics can describe the behavior of such materials and can be used to guide the design of engineered scaled skins with targeted material properties.
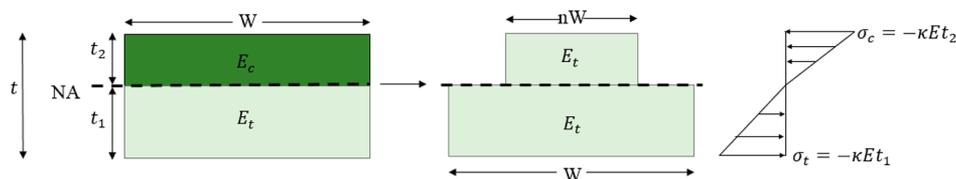
Figure A1. Diagram of the transformed cross section method for the flexural stiffness of foam.

The natural teleost scales, which served as a model for our material, are made of mineralized collagen fibrils that can display remarkable nanomechanics and outstanding properties on their own.[32] A future goal would be to integrate biomimetic fibers with similar properties into the fabrication of the artificial scales. Although the engineered material presented here does not replicate the structural and biochemical complexity of scales and scaled skins in nature, such artificial scaled skins that are flexible, lightweight, transparent, and robust to mechanical deformations may nevertheless find broad application as thin protective coatings or films. As just one example, a bioinspired scaled skin material fabricated from biocompatible components may find application on specialized flexible electronics[33−35] such as surface-mounted tactile probes and implantable biosensors that require durability/wear resistance.

8. APPENDIX: MODELING THE FLEXURAL RESPONSE OF SYNTHETIC FISH SKIN

8.1. Flexural Stiffness of a Foam Specimen

The flexural stiffness of the anisotropic, open-celled, polyurethane foam substrate (153.39 ± 0.01 mm $\times$ 167.87 ± 0.01 mm $\times$ 11.99 ± 0.01 mm) was computed using the method of transformed cross sections, as shown in Figure A1, where n is defined as $n = E_c/E_t$ and $E_c = 0.02$ MPa and $E_t = 0.06$ MPa are the compressive and tensile moduli of the foam, respectively.

Assuming that the net axial strain in the beam cross section was negligible, the neutral axis in the foam specimen was determined by equating the resultant compressive and tensile forces generated during flexure:

$$-\frac{\kappa E_c t_2^2}{2} = -\frac{\kappa E_t t_1^2}{2} \tag{A1}$$

giving

$$NA = \frac{t}{\sqrt{\frac{1}{n} + 1}} \tag{A2}$$

With these results, the moment of inertia of the foam about the lateral axis (abdomen to dorsal side) is given as

$$I_f = \frac{W(NA)^3}{3} + \frac{nW(t - NA)^3}{3} \tag{A3}$$

and the flexural stiffness of the foam is then calculated as $E_t I_f$. Because the measured quantities during testing were load and deflection, rather than load and curvature, the appropriate geometric and constitutive equations were employed to convert total curvature to the deflection of the specimen at the midpoint. Using the classic Timoshenko linear elastic beam theory, the curvature, κ, for every point along the beam is given by solving

$$M(x) = -E_t I_f\left(\frac{d\theta}{dx}\right) = -E_t I_f \kappa \tag{A4}$$

where $M(x) = -Px/2$ as given by simple structural analysis of a point load applied to the center of a simply supported beam. Using a finite difference method, and boundary conditions specified to allow the movement of the beam ends in the x direction and rotation in the y direction, while restricting their vertical deflection in the y direction, the rotation at every point on the beam was calculated. The following equations were then implemented to calculate the new (after deflection) X and Y coordinates of every point on the beam:

$$X(x) = \int_0^{L/2} [1 + \varepsilon(x)] \cos \theta(x) \, dx \tag{A5}$$

$$Y(x) = \int_0^{L/2} [1 + \varepsilon(x)] \sin \theta(x) \, dx \tag{A6}$$

where $\varepsilon(x)$ is the axial strain in the foam calculated by

$$\varepsilon(x) = \frac{\sigma(x)}{E_f}; \ \sigma(x) = \frac{N(x)}{A} \tag{A7}$$

and $N(x)$ is calculated as shown in Figure A2. It was assumed that the axial load was resisted entirely by the foam substrate,
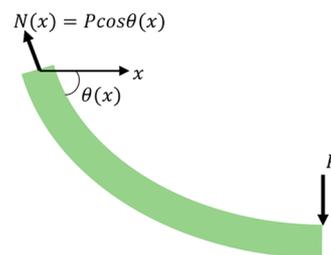
Figure A2. Free-body diagram for calculating beam deformation.

and that deformation from shear was negligible because the foam was relatively thin with respect to its length. With each incrementally applied load, the moment equation from a structural analysis was updated, and the solid green curve in Figure 5a was generated.

8.2. Flexural Stiffness of Synthetic Fish Skin about Its Longitudinal Axis

The flexural response of the synthetic fish skin about the longitudinal axis can be modeled as a composite beam with a solid CAB layer having an effective thickness of 3.2 mm, which is calculated by dividing the total volume of scales used in the specimen by the area that they cover during testing:

$$T_{eff} = \frac{n_s h b l}{W L} \tag{A8}$$

where n_s is the total number scales in the specimen (690) and h, b, and l are the thickness, width, and length of an individual scale, respectively. W and L are the width and length of the foam specimen that the synthetic skin covered during testing, respectively. Because the synthetic skin did not perfectly adhere

to the foam, the internal moment of the specimen is calculated as the sum of the moments generated by the scales and the foam:

$$M(x) = E_t I_f \kappa_f + E_s I_s \kappa_s \tag{A9}$$

where $E_t I_f$ is the flexural stiffness of the foam as calculated above, E_s is the modulus of elasticity of the CAB sheet (800 MPa), and I_s is the moment of inertia of the scales given as $I_s = [L(T_{eff})^3]/12$ For the sake of simplifying this equation, the curvature of the foam can be related to the curvature of the scales through the following equation:

$$\kappa_f = \frac{1}{\frac{1}{\kappa_s} + 0.5T_{eff} + (t - NA)} \tag{A10}$$

With this equation, it was possible to solve for the curvature of the scales, κ_s, and then use the relation described in section 8.1 to solve for the deflection of the beam.

8.3. Flexural Stiffness of Synthetic Fish Skin about Its Lateral Axis

The energy associated with fish skin curvature can be decomposed into rotational and bending energies.[12] The rotational energy is described as the energy stored by the skin "pockets" as scales rotate about the lateral axis. The pockets act as rotational springs, thus resisting out-of-plane deformation. For small pocket stiffness, scale rotation is predominant as the skin first begins to bend, allowing relatively large flexural deformations for a relatively small moment. As the curvature increases, geometrical constraints force the scales to bend, causing a stiffening in the flexural moment response. Individual scales store this component of the bending energy. Together, these two mechanisms induce the overall flexural response in fish skin, as shown in Figure 5d. Adopting this energy decomposition and invoking the principle of energy minimization, we have shown that the internal moment in the scaled skin can be computed as

$$M = \frac{(EI)_s}{rl}[\bar{\kappa} - \bar{\kappa}_r(\bar{\kappa})] \tag{A11}$$

where El_s is the bending stiffness of a single scales, r and l are the geometric parameters as seen in Figure 5d, and $\bar{\kappa}$ and $\bar{\kappa}_r$ are the normalized total curvature and the curvature generated by scale rotation, respectively.[12] These curvatures are normalized by the length of a single scale, l (e.g., $\bar{\kappa} = lk$). For the full derivation of eq A11, see ref 12. Here, this derivation is combined with a general large deformation bending model (eq A12) for a composite beam composed of an upper scaled layer and a lower polyurethane foam layer. The flexural stiffness associated with the polyurethane foam was computed as described in section 8.1. The total external moment generated by the applied load was considered to be equal to the sum of the internal moments of the scales and the foam:

$$M(x) = E_t I_f \bar{\kappa}_f + \frac{(EI)_s}{rl}[\bar{\kappa} - \bar{\kappa}_r(\bar{\kappa})] \tag{A12}$$

where

$$\bar{\kappa}_f = \frac{1}{\frac{1}{\bar{\kappa}} + (t - NA)} \tag{A13}$$

is the curvature of the foam about the neutral axis, computed with respect to the curvature of the scales and $E_t I_f$ is the flexural

stiffness of the foam. To solve this equation, the first step is to show with a simple structural analysis that

$$M(x) = \frac{Px}{2} \tag{A14}$$

Substituting the following equation from the derivation of Vernerey and Barthelat,[12] we can simplify this expression further:

$$\bar{\kappa} = \bar{\kappa}_r + \bar{K}\theta(\bar{\kappa}_r)\theta'(\bar{\kappa}_r) \tag{A15}$$

Transforming eq A12 into

$$EI_f\left[\frac{1}{\frac{1}{\bar{\kappa}_r + \bar{K}\theta(\bar{\kappa}_r)\theta'(\bar{\kappa}_r)} + (t - NA)}\right] + \frac{(EI)_s}{rl}$$
$$[\bar{\kappa}_r + \bar{K}\theta(\bar{\kappa}_r)\theta'(\bar{\kappa}_r)] - \frac{Px}{2}$$
$$= 0 \tag{A16}$$

where

$$\theta(\bar{\kappa}_r) = \frac{-r\bar{\kappa}_r}{2} + \sin^1\left[\bar{\kappa}_r \cos\left(\frac{r\bar{\kappa}_r}{2}\right)\right] \tag{A17}$$

and

$$\theta'(\bar{\kappa}_r) = \frac{-r}{2} + \frac{\cos\left(\frac{r\bar{\kappa}_r}{2}\right) - \frac{r\bar{\kappa}_r}{2}\sin\left(\frac{r\bar{\kappa}_r}{2}\right)}{\sqrt{1 - \left[\bar{\kappa}_r \cos\left(\frac{r\bar{\kappa}_r}{2}\right)\right]^2}} \tag{A18}$$

The normalized rotational curvature can be found numerically by using the Newton−Raphson algorithm, and in turn, the total normalized curvature can be found using eq A15. This quantity is then transformed into the actual curvature by dividing by the length of a scale l. Once the value for curvature at every point along the beam had been determined, the relations described in section 8.1 were used to determine the deflection of the beam.

AUTHOR INFORMATION

Corresponding Authors
*E-mail: mark.stoykovich@colorado.edu.
*E-mail: franck.vernerey@colorado.edu.

Notes
The authors declare no competing financial interest.

REFERENCES

(1) Chen, I. H.; Kiang, J. H.; Correa, V.; Lopez, M. I.; Chen, P.-Y.; McKittrick, J.; Meyers, M. A. Armadillo Armor: Mechanical Testing and Micro-structural Evaluation. *J. Mech. Behav. Biomed. Mater.* **2011**, *4*, 713−722.

(2) Raabe, D.; Sachs, C.; Romano, P. The Crustacean Exoskeleton as an Example of a Structurally and Mechanically Graded Biological Nanocomposite Material. *Acta Mater.* **2005**, *53*, 4281−4292.

(3) Elliott, D. G. In *The Laboratory Fish*; Ostrander, G. K., Ed.; Academic Press: San Diego, 2000; Chapter 5, p 99.

(4) Zhu, D.; Szewciw, L.; Vernerey, F.; Barthelat, F. Puncture Resistance of the Scaled Skin from Striped Bass: Collective Mechanisms and Inspiration for New Flexible Armor Designs. *J. Mech. Behav. Biomed. Mater.* **2013**, *24*, 30−40.

(5) Ikoma, T.; Kobayashi, H.; Tanaka, J.; Walsh, D.; Mann, S. Microstructure, Mechanical, and Biomimetic Properties of Fish Scales from *Pagrus major*. *J. Struct. Biol.* **2003**, *142*, 327−333.

(6) Meunier, F. J.; Castanet, J. Organisation Spatiale des Fibres de Collagène de la Plaque Basale des écailles des Téléostéens. *Zool. Scr.* **1982**, *11*, 141−153.

(7) Vickaryous, M. K.; Sire, J.-Y. The Integumentary Skeleton of Tetrapods: Origin, Evolution, and Development. *J. Anat.* **2009**, *214*, 441−464.

(8) Zylberberg, L.; Bonaventure, J.; Cohen-Solal, L.; Hartmann, D. J.; Bereiter-Hahn, J. Organization and Characterization of Fibrillar Collagens in Fish Scales in situ and in vitro. *J. Cell Sci.* **1992**, *103*, 273−285.

(9) Yang, W.; Chen, I. H.; Gludovatz, B.; Zimmermann, E. A.; Ritchie, R. O.; Meyers, M. A. Natural Flexible Dermal Armor. *Adv. Mater. (Weinheim, Ger.)* **2013**, *25*, 31−48.

(10) Lin, Y.-S.; Wei, C. T.; Olevsky, E. A.; Meyers, M. A. Mechanical Properties and the Laminate Structure of *Arapaima gigas* Scales. *J. Mech. Behav. Biomed. Mater.* **2011**, *4*, 1145−1156.

(11) Chen, P. Y.; Schirer, J.; Simpson, A.; Nay, R.; Lin, Y.-S.; Yang, W.; Lopez, M. I.; Li, J. N.; Olevsky, E. A.; Meyers, M. A. Predation versus Protection: Fish Teeth and Scales Evaluated by Nano-indentation. *J. Mater. Res.* **2012**, *27*, 100−112.

(12) Vernerey, F. J.; Barthelat, F. Skin and Scales of Teleost Fish: Simple Structure but High Performance and Multiple Functions. *J. Mech. Phys. Solids* **2014**, *68*, 66−76.

(13) Browning, A.; Ortiz, C.; Boyce, M. C. Mechanics of Composite Elasmoid Fish Scale Assemblies and their Bioinspired Analogues. *J. Mech. Behav. Biomed. Mater.* **2013**, *19*, 75−86.

(14) Whitear, M. In *Biology of the Integument*; Bereiter-Hahn, J., Matoltsy, A. G., Richards, K. S., Eds.; Springer-Verlag: Berlin, 1986; Chapter 2, pp 8−38.

(15) Zhu, D.; Ortega, C. F.; Motamedi, R.; Szewciw, L.; Vernerey, F.; Barthelat, F. Structure and Mechanical Performance of a "Modern" Fish Scale. *Adv. Eng. Mater.* **2012**, *14*, B185−B194.

(16) Torres, F. G.; Troncoso, O. P.; Nakamatsu, J.; Grande, C. J.; Gomez, C. M. Characterization of the Nanocomposite Laminate Structure Occurring in Fish Scales from *Arapaima gigas*. *Mater. Sci. Eng., C* **2008**, *28*, 1276−1283.

(17) Bruet, B. J. F.; Song, J. H.; Boyce, M. C.; Ortiz, C. Materials Design Principles of Ancient Fish Armour. *Nature* **2008**, *7*, 748−756.

(18) Meyers, M. A.; Lin, Y. S.; Olevsky, E. A.; Chen, P.-Y. Battle in the Amazon: *Arapaima* versus *Piranha*. *Adv. Eng. Mater.* **2012**, *14*, B279−B288.

(19) Long, J. H.; Hale, M. E.; Henry, M. J. M. C.; Westneat, M. W. Functions of Fish Skin: Flexural Stiffness and Steady Swimming of Longnose Gar, *Lepisosteus osseus*. *J. Exp. Biol.* **1996**, *199*, 2139−2151.

(20) Song, J. Multiscale Materials Design of Natural Exoskeletons: Fish Armor. Ph.D. Thesis, Massachusetts Institute of Technology, Cambridge, MA, 2011.

(21) Reichert, S. H. Reverse Engineering Nature: Design Principles for Flexible Protection Inspired by Ancient Fish Armor of Polypteridae. M.S. Thesis, Massachusetts Institute of Technology, Cambridge, MA, 2010.

(22) Kim, S.; Su, Y.; Mihi, A.; Lee, S.; Liu, Z.; Bhandakkar, T. K.; Wu, J.; Geddes, J. B.; Johnson, H. T.; Zhang, Y.; Park, J.-K.; Braun, P. V.; Huang, Y.; Rogers, J. A. Imbricate Scales as a Design Construct for Microsystem Technologies. *Small* **2012**, *8*, 901−906.

(23) Chintapalli, R. K.; Mirkhalaf, M.; Dastjerdi, A. K.; Barthelat, F. Fabrication, Testing and Modeling of a New Flexible Armor Inspired from Natural Fish Scales and Osteoderms. *Bioinspiration Biomimetics* **2014**, *9*, 036005.

(24) Hansen, K. A.; Weiss, J. A.; Barton, J. K. Recruitment of Tendon Crimp with Applied Tensile Strain. *J. Biomech. Eng.* **2002**, *124*, 72−77.

(25) Dobrzański, L. A.; Król, M.; Bilewicz, M.; Viana, J. C. Microstructure and Mechanical Properties of Polypropylene/Poly-carbonate Blends. *Journal of Achievements in Materials and Manufacturing Engineering* **2008**, *27*, 19−22.

(26) Vernerey, F.; Pak, R. Y. S. Analysis of Soft Fibers with Kinematic Constraints and Cross-Links by Finite Deformation Beam Theory. *J. Eng. Mech.* **2011**, *137*, 527−536.

(27) Hebrank, M. R.; Hebrank, J. H. The Mechanics of Fish Skin: Lack of an External Tendon Role in 2 Teleosts. *Biol. Bull. (Woods Hole, MA, U.S.)* **1986**, *177*, 236−247.

(28) Vernerey, F. J.; Barthelat, F. On the Mechanics of Fishscale Structures. *Int. J. Solids Struct.* **2010**, *47*, 2268−2275.

(29) Dobb, M. G.; Johnson, D. J.; Saville, B. P. Supramolecular Structure of a High-Modulus Polyaromatic Fiber (Kevlar 49). *J. Polym. Sci., Part B: Polym. Phys.* **1977**, *15*, 2201−2211.

(30) Treacy, M. M. J.; Ebbesen, T. W.; Gibson, J. M. Exceptionally High Young's Modulus Observed for Individual Carbon Nanotubes. *Nature* **1996**, *381*, 678−680.

(31) Vigolo, B.; Penicaud, A.; Coulon, C.; Saunder, C.; Pailler, R.; Journet, C.; Bernier, P.; Poulin, P. Macroscopic Fibers and Ribbons of Oriented Carbon Nanotubes. *Science* **2000**, *290*, 1331−1334.

(32) Buehler, M. J. Nature Designs Tough Collagen: Explaining the Nanostructure of Collagen Fibrils. *Proc. Natl. Acad. Sci. U.S.A.* **2006**, *103*, 12285−12290.

(33) Rogers, J. A.; Someya, T.; Huang, Y. Materials and Mechanics for Stretchable Electronics. *Science* **2010**, *327*, 1603−1607.

(34) Ko, H. C.; Stoykovich, M. P.; Song, J.; Malyarchuk, V.; Choi, W. M.; Yu, C. J.; Geddes, J. B.; Xiao, J.; Wang, S.; Huang, Y.; Rogers, J. A. A Hemispherical Electronic Eye Camera based on Compressible Silicon Optoelectronics. *Nature* **2008**, *454*, 748−753.

(35) Kim, D. H.; Viventi, J.; Amsden, J. J.; Xiao, J. L.; Vigeland, L.; Kim, Y. S.; Blanco, J. A.; Panilaitis, B.; Kaplan, D. L.; Omenetto, F. G.; Huang, Y. G.; Hwang, K. C.; Zakin, M. R.; Litt, B.; Rogers, J. A. Dissolvable Films of Silk Fibroin for Ultrathin Conformal Bio-integrated Electronics. *Nat. Mater.* **2010**, *9*, 511−517.